PERGAMON

International Journal of Solids and Structures 40 (2003) 5017–5035

INTERNATIONAL JOURNAL OF SOLIDS and STRUCTURES

www.elsevier.com/locate/ijsolstr

Dynamic non-linear behavior and stability of a ventricular assist device

Paulo B. Gonçalves [a,*], Djenane Pamplona [a], Pedro B.C. Teixeira [a], Renato L.C. Jerusalmi [a], Idágene A. Cestari [b], Adolfo A. Leirner [b]

[a] *Department of Civil Engineering, Pontifical Catholic University, PUC-Rio, Rua Mq. São Vicente 225, 22453-900 Rio de Janeiro, Brazil*

[b] *Center of Biomedical Technology, Heart Institute (InCor), University of São Paulo Medical School, 05403-000 São Paulo, Brazil*

Received 12 September 2002; received in revised form 8 January 2003

Abstract

This paper investigates the non-linear dynamic behavior and stability of the internal membrane of a ventricular assist device (VAD). This membrane separates the blood chamber from the pneumatic chamber, transmitting the driving cyclic pneumatic loading to blood flowing from the left ventricle into the aorta. The membrane is a thin, nearly spherical axi-symmetric shallow cap made of polyurethane and reinforced with a cotton mesh. Experimental evidence shows that the reinforced membrane behaves as an isotropic elastic material and exhibits both membrane and flexural stiffness. So, the membrane is modeled as an isotropic pressure loaded shallow spherical shell and its dynamic behavior and snap-through buckling considering different types of dynamic excitation relevant to the understanding of the VAD behavior is investigated. Based on Marguerre kinematical assumptions, the governing partial differential equations of motion are presented in the form of a compatibility equation and a transverse motion equation. The results show that the shell, when subjected to compressive pressure loading, may loose its stability at a limit point, jumping to an inverted position. If the compressive load is removed, the shell jumps back to its original configuration. This non-linear behavior is the key feature in the VAD behavior.

Keywords: Ventricular assist device (VAD); Artificial organs; Dynamic buckling; Shallow spherical shells; Non-linear oscillations; Snap-through buckling; Dynamic bifurcations

1. Introduction

Statistics have shown that nowadays the number of deaths by congestive cardiac failure is greater then the deaths by breast cancer and AIDS together. Recent studies reveals that only in the United States cardiac transplant and mechanical assist devices could be profitable to over 60,000 patients every year. In Brazil the perspectives are even worse because of Chagas disease. Heart transplants have become a routine procedure

* Corresponding author. Tel.: +55-21-3114-1188/3114-1189; fax: +55-21-3114-1195.
E-mail address: paulo@civ.puc-rio.br (P.B. Gonçalves).

0020-7683/$ - see front matter © 2003 Elsevier Ltd. All rights reserved.
doi:10.1016/S0020-7683(03)00252-X

in many medical centers during the past 25 years. Approximately 2200 heart transplants are carried out each year in the United States only. Most transplant patients enjoy a full active life, and some can even return to full-time employment. However, there is a shortage of hearts for donation and a large number of patients waiting for a transplant die before a suitable donor becomes available. A weakness in the left ventricle is the cause of heart failure in most patients. In these circumstances, the use of a ventricular assist device (VAD) is of fundamental importance to assist the patients while they wait for a donor in case their condition makes survival impossible, despite maximal pharmacological therapy. VAD is a heart pump that can be used to substitute temporarily the left ventricle, the main chamber of the heart. This use is called bridge to transplant. There are also some cases where mechanical support will cause a return to normal function and thus avoid transplantation. In Brazil, the Heart Institute, InCor-SP, is developing a pneumatically actuated, free-floating membrane VAD that has been shown to be a valuable device to increase the life span of patients with congestive cardiac failure (Leiner et al., 1998; Sezai, 2001). This VAD is basically a rigid container with two chambers: a pneumatic chamber, connected to a pump, and the blood chamber, connecting the left ventricle to the aorta. A thin walled shallow moving membrane, as illustrated in Fig. 1 separates these two chambers. A photograph of a VAD prototype cut in half is shown in Fig. 2, where one can see all its parts. This shallow membrane plays an important role in the mechanical operation of the VAD–InCor, as shown herein.

This membrane is a thin nearly spherical axi-symmetric membrane made of polyurethane and reinforced with a cotton net, as shown in Fig. 3(a). Fig. 3(b) shows the membrane within the VAD prototype. The purpose of this cotton net is to decrease the strains of the membrane, thus avoiding the contact of the membrane with the chamber wall, which would provoke hemolysis.An experimental program was conducted recently (Teixeira, 2001; Teixeira et al., 2001) and it was observed that this reinforced membrane behaves under the present circumstances as an isotropic material and exhibits both membrane and flexural stiffness. So, based on these results and the mechanical model, this paper models the membrane as a shallow, spherical isotropic shell, clamped along the edge and subjected to hydrostatic pressure. The total

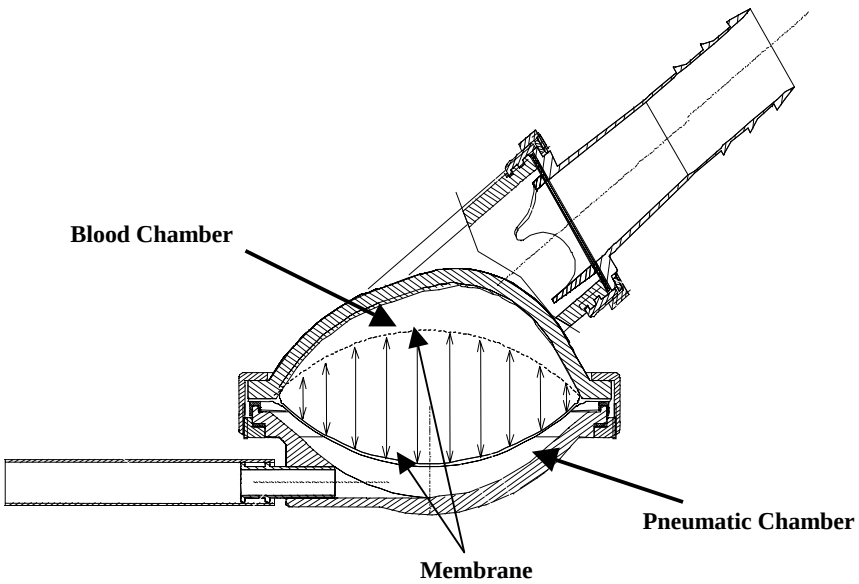

Fig. 1. Schematic illustration of the VAD, showing the two possible equilibrium states of the membrane (pre- and post-buckling positions).

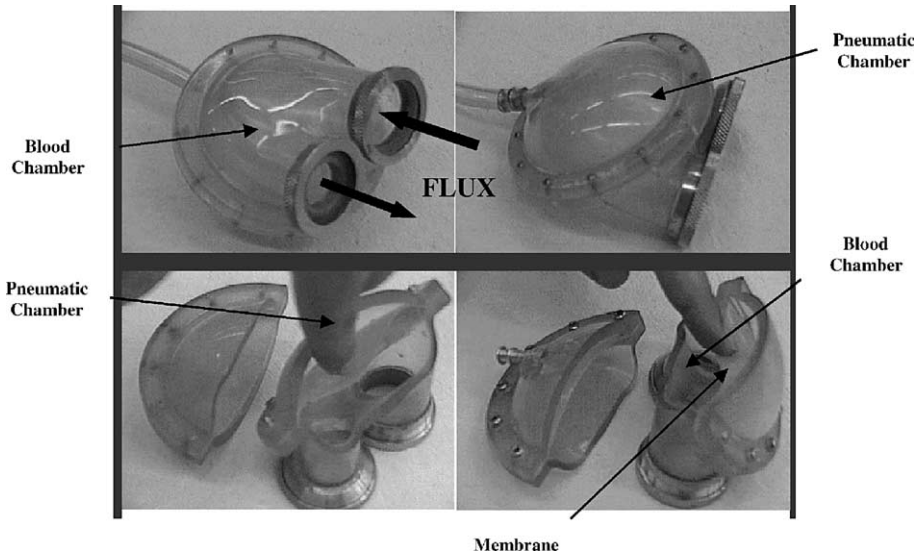

Fig. 2. VAD prototype.

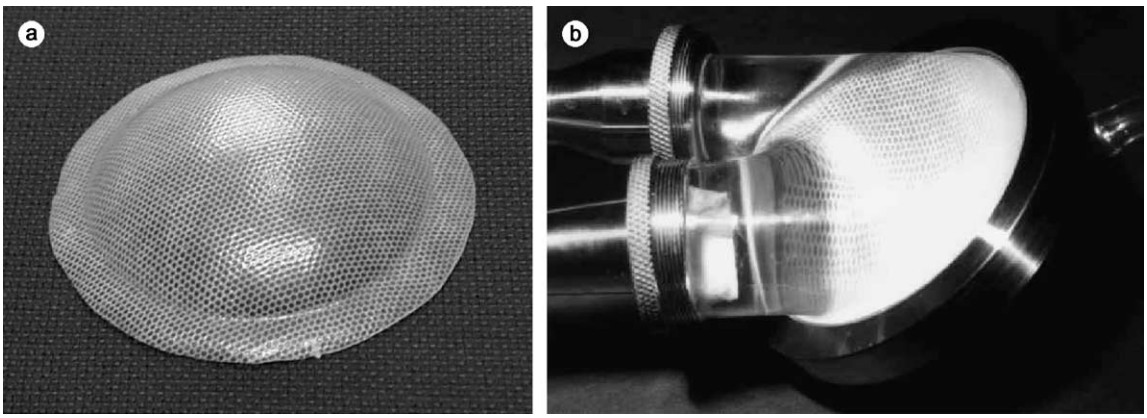

Fig. 3. VAD internal reinforced membrane.

hydrostatic pressure is the difference between the pneumatic pressure and the blood pressure. The static stability analysis of pressure-loaded spherical shells has been the subject of several papers in the past; see, for example, Tillman (1970), Yamada et al. (1983) and Gonçalves and Croll (1992). These studies show that, under pressure loading, shallow spherical shells exhibit a highly non-linear behavior and, when subjected to compressive pressure loading, may lose their stability at a limit point, jumping to an inverted position. This phenomenon is known in structural engineering as snap-through buckling. If the compressive load is removed, the shell jumps back to its original configuration. These studies have also shown that the critical load is highly dependent on load and geometric imperfections. This non-linear behavior is the key feature in the behavior of the VAD. As the shell jumps to an inverted position, it transmits the pneumatic load to the blood that has entered the blood chamber, expelling it. When the pneumatic load is removed the shell snaps back and new blood enters the blood chamber, thus making the desired blood flow possible (see

Fig. 1). Therefore the performance, reliability and durability of the membrane are critical for the full functioning of the VAD. Recently the authors presented an analytical and experimental study of the static behavior and stability of the inner membrane of the VAD–InCor (Teixeira et al., 2001). In this study the authors obtained the physical characteristics of the VAD membrane and studied the influence of shell geometry, load and geometric imperfections on the non-linear behavior and stability of the cap. The results show clearly the main characteristics of the VAD behavior and also the high imperfection sensitivity of the critical load on the degree and type of imperfections. This study was performed using both the Marguerre's non-linear shallow shell equations and the finite element software ABAQUS (Hibbitt, 1998).

However, the snap-through buckling is eminently a dynamic phenomenon. Also, as the load repeats itself in order to make the blood flow possible, the shell exhibits a large cross-well motion, jumping from one equilibrium position to another. So in order to understand completely the VAD behavior and avoid possible dynamic instabilities which may cause undesirable pressure fluctuations, a detailed analysis of the non-linear dynamic behavior of the VAD membrane is still necessary.

The dynamic stability analysis of spherical caps has not received much attention from investigators, possibly because of the difficulties in approaching this problem in a systematic manner, and criteria for dynamic buckling are not well established (Budiansky and Hutchinson, 1964). Moreover most of the studies on the axi-symmetric dynamic buckling of shallow spherical caps have focused their attention on the snap-through buckling under a step load of infinite duration (Budiansky and Roth, 1962; Huang, 1969; Simitses, 1974; Dumir et al., 1984). However recent studies have shown that (Gonçalves, 1999; Soliman and Gonçalves, 2003) these shells may display, due to its inherently non-linear nature, sub-harmonic and superharmonic oscillations, period-multiplying bifurcations, multiple solutions, chaotic motions and jumps due to the presence of competing potential wells and non-linear resonance curves within each well. So, in the design of the VAD special attention should be given to the phenomenon of *escape* from the potential well associated with the pre-buckling solution (Thompson, 1989; Virgin et al., 1992). For small forcing amplitudes, the motions remain in the neighborhood of the static non-linear reference state, confined into the pre-buckling well; but, for certain critical values of the control parameters, the motion can no longer be confined into this well and the shell jumps into another well or may exhibit large cross-well motions. These critical values may be smaller than the corresponding static buckling load and the reduction in the load carrying capacity depends upon the characteristics of the dynamic load and shell imperfections. So, in order to design such a system, one must understand the physical process involved in non-linear dynamic buckling and, from this knowledge, devise clear criteria and estimates for critical conditions.

In the present work accurate non-linear modeling for the axi-symmetric dynamic behavior of clamped shallow spherical shells is presented, which considers the combined effects of pressure loading and geometric imperfections on the vibration characteristics and non-linear response of the cap under dynamic excitation. The basic approach in this work is to solve the dynamic version of the fourth-order Marguerre equations by the Galerkin method. An accurate solution described by a linear combination of Bessel functions and modified Bessel functions based on the free vibration modes of the unloaded perfect cap (Yasuda and Kushida, 1984; Gonçalves, 1994) is used to determine the non-linear pre-stress state of the imperfect cap and to examine its non-linear vibration characteristics along the pre- and post-buckling paths. Each term of the modal expansions satisfies all the relevant boundary and continuity conditions.

2. Basic equations

The geometry of a uniformly loaded shallow spherical cap with clamped edge conditions is presented in Fig. 4, where R, a, H and h are the principal radius of curvature of the sphere, the base radius of the cap, the rise of the mid-surface at the apex and the shell thickness, respectively. The polar co-ordinate system in the

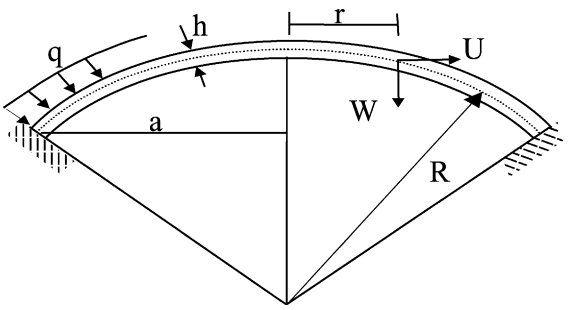

Fig. 4. Shell geometry and co-ordinate system.

base plane is defined by r and θ, and the uniform pressure distributed over the surface of the shell is denoted by q.

Within the framework of shallow shell theory ($H/a < 0.25$), the tangential forces and displacements can be taken to be their projections onto the base plane of the shell. Marguerre (1939) formulated the basic equations governing moderately large displacements and rotations, but small strains, of shallow spherical caps. In the case of axi-symmetric static deformations of a thin imperfect cap, the governing equations may be expressed in the non-dimensional form as

$$\nabla^4 w_s = \lambda^2 \alpha^{1/2} \nabla^2 f_s + Q \frac{4\lambda^4}{\alpha^{1/2}} + \frac{\alpha}{x}\{f_{s,x}(w_{s,x} + \hat{w}_{,x})\}_{,x}, \tag{1a}$$

$$\nabla^4 f_s = -\lambda^2 \alpha^{-1/2} \nabla^2 w_s - \frac{1}{x}\{w_{s,x} w_{s,xx} + (\hat{w}_x w_{s,x})_{,x}\}, \tag{1b}$$

where $(\cdot)_{,x} = \partial(\cdot)/\partial x$, $\alpha = 12(1 - v^2)$ and λ is a geometrical parameter described by

$$\lambda = \alpha^{1/4} a / \sqrt{\mathrm{Rh}}. \tag{2}$$

The non-dimensional radial co-ordinate x, the vertical displacement w_s, imperfection shape $\hat{w}$, stress function f_s, and load parameter Q are related to the corresponding physical quantities by the following relations

$$x = \frac{r}{a}, \quad w_s = \frac{W_s}{h}, \quad \hat{w} = \frac{\hat{W}}{h}, \quad f_s = \frac{F_s}{Eh^3}, \quad Q = \frac{q}{q_{\mathrm{cl}}}, \tag{3}$$

where $q_{\mathrm{cl}} = 2E(h/R)^2/\sqrt{3(1 - v^2)}$ is the classical buckling pressure of a complete spherical shell, E is the Young's modulus and v is the Poisson's ratio.

The static stress resultants, couples and non-linear strain–displacement relations are given by

$$\begin{aligned}
&\frac{a^2 N_r}{Eh^3} = \frac{1}{x} f_{s,x}; \quad \frac{a^2 N_\theta}{Eh^3} = \frac{1}{x} f_{s,xx}, \\
&\frac{12(1 - v^2) a^2 M_r}{Eh^4} = \frac{1}{x} w_{s,x} + v w_{s,xx}; \quad \frac{12(1 - v^2) a^2 M_\theta}{Eh^4} = \frac{1}{x} w_{s,xx} + v w_{s,x}, \\
&\varepsilon_r = \frac{h}{a} u_{s,x} + \left(\frac{h}{a}\right)^2 \left[\hat{w}_{,x} w_{s,x} + \frac{1}{2} w_{s,x}^2\right]; \quad \varepsilon_\theta = \frac{h}{a} \frac{u_s}{x},
\end{aligned} \tag{4}$$

where $u_s (= U_s/h)$ is the non-dimensional displacement in the radial direction.

The boundary conditions at the clamped edge $x = 1$ of the shallow shell are

$$w_s = 0, \quad w_{s,x} = 0, \quad u_s = f_{s,xx} - \frac{v}{x} f_{s,x} = 0. \tag{5a}$$

Additionally, the following restrictions must be imposed at $x = 0$

$$w_s = 0, \quad f = 0. \tag{5b}$$

When a uniform static pressure is applied to the cap, it yields a basic static geometrically non-linear state of displacements and stresses. To represent the basic static axi-symmetric response, the displacement w_x and the stress function f_x are assumed in the form

$$w_s(x) = \sum_{i=1}^{\mathrm{NS}} W_{0i}\phi_i(x), \tag{6a}$$

$$f_s(x) = \sum_{i=1}^{\mathrm{NS}} F_{0i}\psi_i(x), \tag{6b}$$

where each separate generalized function

$$\phi_i(x) = J_0(K_i x) + \frac{J_1(K_i)}{I_1(K_i)} I_0(K_i x) - \left[J_1(K_i)\frac{I_0(K_i)}{I_1(K_i)} + J_0(K_i) \right], \tag{7a}$$

$$\psi_i(x) = J_0(K_i x) + \frac{J_1(K_i)}{I_1(K_i)} I_0(K_i x) + \frac{K_i^2(\lambda^4 + K_i^4)}{4\lambda^4} \left[J_1(K_i)\frac{I_0(K_i)}{I_1(K_i)} + J_0(K_i) \right] x^2, \tag{7b}$$

exactly satisfies the clamped boundary conditions at $x = 1$ as well as the continuity requirements of displacements and stresses at the center of the shell ($x = 0$).

In Eqs. (7a) and (7b) J_0 and J_1 are Bessel functions, and I_0, and I_1 modified Bessel functions of the first kind, and K_n $(0 < K_1 < K_2 < \cdots)$ are the roots of the equation

$$[J_0(K_n)I_1(K_n) + I_0(K_n)J_1(K_n)]K_n \left[\frac{\lambda^4 + K_n^4}{\lambda^4} \frac{(1-v)}{2} - 1 \right] + 2J_1(K_n)I_1(K_n)(1+v) = 0. \tag{8}$$

It might be observed that the generalized functions (7a) and (7b) are also the linear vibration modes of an unloaded clamped shallow spherical shell (Yasuda and Kushida, 1984).

To facilitate a convenient representation of axi-symmetric geometric imperfections of an arbitrarily specified shape and consequently allow an efficient modal analysis of the imperfect shell, a Fourier–Bessel series is used to describe the "general" imperfection, $\hat{w}(x)$. This Fourier–Bessel series may be written as

$$\hat{w}(x) = \hat{W}^0_{\mathrm{MAX}} \left[\sum_{i=1}^{\mathrm{NI}} \hat{w}_i \phi_i(x) \Big/ \mathrm{MAX}\left(\sum_{i=1}^{\mathrm{NI}} \hat{w}_i \phi_i(x) \right) \right], \tag{9}$$

where $\hat{w}_i$ is the amplitude of the ith harmonic and $\phi_i(x)$ is the modal function given by (7a). Note that $\{\phi_i(x)\}$ represents a complete set of orthogonal functions in [0,1] (Yasuda and Kushida, 1984).

For convenience, the expression between bracket in (9) is written in such a way its maximum value is always equal to one. Consequently the magnitude and sign of the maximum amplitude will be given by $\hat{W}^0_{\mathrm{MAX}}$.

Substituting expressions (6) and (9) into Eqs. (1a) and (1b) and applying a Galerkin minimization procedure one obtains the following set of 2NS non-linear algebraic equations characterizing the static behavior of the cap:

$$W_{0n}K_n^4/2\{A(K_n)-[2J_1(K_n)B(K_n)/K_n]\}+\bar{F}_{0n}\{[(2\lambda^4+K_n^4)/2]A(K_n)-[J_1(K_n)(3\lambda^4+2K_n^4)B(K_n)/K_n]$$
$$+(\lambda^4+K_n^4)C(K_n)\}+\sum_{\substack{i=1\\(i\neq n)}}^{\mathrm{NS}}\{\{2W_{0i}K_n^3K_i^3[K_iJ_1(K_n)B(K_i)-K_nJ_1(K_i)B(K_n)]/(K_n^4-K_i^4)\}$$
$$+F_{01}\{[2\lambda^4K_n^3[J_1(K_n)B(K_i)-(K_n/K_i)J_1(K_i)B(K_n)]/(K_n^4-K_i^4)]$$
$$+(\lambda^4+K_i^4)B(K_i)B(K_n)/2-2J_1(K_n)/K_n]\}\}Q[4\lambda^4\alpha^{-1/2}][2J_1(K_n)/K_n-B(K_n)/2]$$
$$+\sum_{i=1}^{\mathrm{NS}}\sum_{j=1}^{\mathrm{NS}}\alpha^{1/2}\lambda^2W_{0i}\bar{F}_{0j}K_i\alpha_{ijn}+\sum_{i=1}^{\mathrm{NS}}\sum_{j=1}^{\mathrm{NS}}\alpha^{1/2}\lambda^2\hat{W}_i\bar{F}_{0j}K_i\alpha_{ijn}=0;\quad n=1,\mathrm{NS},\tag{10}$$

$$(\bar{F}_0n-W_{0n})\{[(2\lambda^4+K_n^4)A(K_n)/2]+(\lambda^4+K_n^4)C(K_n)-[(3\lambda^4+2K_n^4)J_1(K_n)B(K_n)/K_n]\}$$
$$+\sum_{\substack{(i=1)\\(i\neq n)}}^{\mathrm{NS}}(\bar{F}_i-W_i)\{(\lambda^4+K_n^4)B(K_n)[B(K_i)/2-2J_1(K_i)/K_i]+\{2\lambda^4K_i^3[J_1(K_n)K_iB(K_i)/K_n$$
$$-J_1(K_i)B(K_n)]/(K_n^4-K_i^4)\}\}+\sum_{i=1}^{\mathrm{NS}}\sum_{j=1}^{\mathrm{NS}}\alpha^{1/2}\lambda^2W_{01}W_{0j}K_iK_j^2\beta_{ijn}/K_n^2$$
$$+\sum_{i=1}^{\mathrm{NS}}\sum_{j=1}^{\mathrm{NS}}\alpha^{1/2}\lambda^2\hat{W}_1W_{0j}K_iK_j^2\beta_{ijn}/K_n^2\sum_{i=1}^{\mathrm{NS}}\sum_{j=1}^{\mathrm{NS}}\alpha^{1/2}\lambda^2W_{0i}\hat{W}_jK_iK_j^2\beta_{ijn}/K_n^2=0;\quad n=1,\mathrm{NS},\tag{11}$$

where $\bar{F}_{0k}=F_{0k}\alpha^{1/2}/\lambda^2$, $\hat{W}_i=\hat{W}^0_{\mathrm{MAX}}\hat{w}_i$ and

$$\begin{aligned}A(K_n)&=J_0^2(K_n)+J_1^2(K_n)[I_0(K_n)/I_1(K_n)]^2,\\B(K_n)&=J_0(K_n)+J_1(K_n)[I_0(K_n)/I_1(K_n)],\\C(K_n)&=J_0(K_n)+J_1(K_n)I_0(K_n)/I_1(K_n).\end{aligned}\tag{12}$$

In the numerical computations for this problem it is necessary to estimate the constants α_{ijn} and β_{ijn}. They are integrals involving products of Bessel functions and modified Bessel functions for which there are no closed form solutions. Here they were computed using the polynomial expansions presented by Abramovitz and Stegun (1964) and the 11 point Newton–Cotes formula with four hundred values over the range of the integrand. These integrals are of the form

$$\alpha_{ijn}=\int_0^1\{\{D(K_i)[(K_i/K_j)BI(K_ix)J_1(K_jx)+I_1(K_ix)BJ(K_jx)]+D(K_i)D(K_j)[(K_i/K_j)BI(K_ix)I_1(K_jx)$$
$$+I_1(K_ix)BI(K_jx)]-D(K_i)C(K_j)[K_iBI(K_ix)x+I_1(K_ix)]-[(K_i/K_j)BJ(K_ix)J_1(K_jx)$$
$$+J_1(K_jx)BJ(K_jx)]-D(K_i)[(K_i/K_j)BJ(K_ix)I_1(K_jx)+J_1(K_ix)BI(K_jx)]$$
$$+C(K_j)[K_iBJ(K_ix)x+J_1(K_ix)]\}\{J_0(K_nx)+D(K_n)I_0(K_nx)-C(K_n)\}\}\mathrm{d}x,\tag{13}$$

where

$$\begin{aligned}BI(K_ix)&=I_0(K_ix)-(1/K_ix)I_1(K_ix),\\BJ(K_ix)&=J_0(K_ix)-(1/K_ix)J_1(K_ix),\\C(K_i)&=J_1(K_i)[I_0(K_i)/I_1(K_i)]+J_0(K_i),\\D(K_i)&=J_1(K_i)/I_1(K_i)\end{aligned}\tag{14}$$

and

$$\beta_{ijn} = \int_0^1 \{\{D(K_i)D(K_j)I_1(K_ix)BI(K_jx) - D(K_i)I_1(K_ix)BJ(K_jx)D(K_j)J_1(K_ix)BI(K_jx) + J_1(K_ix)BJ(K_jx)\{J_0(K_nx) - D(K_n)I_0(K_nx) + E(K_n)x^2\}\}\}\mathrm{d}x, \tag{15}$$

where

$$E(K_n) = \frac{K_n^2(\lambda^4 + K_n^4)}{4\lambda^4} C(K_n). \tag{16}$$

The expressions (7a) and (7b) are used as the weighting functions in this Galerkin procedure. These algebraic non-linear equations are solved by the Newton–Raphson method together with path following strategies.

In the further analysis the dynamic behavior of the cap around the axi-symmetric non-linear static state will be considered. For this, a dynamic perturbation is superimposed on the basic static state. In this case one has

$$\begin{aligned} W_p(x,t) &= \hat{w}(x) + w_s(x) + w(x,t), \\ F_p(x,t) &= f_s(x) + f(x,t), \end{aligned} \tag{17}$$

where $w(x,t)$ denotes the incremental displacement component and $f(x,t)$ the corresponding incremental stress function.

Using expressions (17) and the dimensionless parameters, one obtains the following non-dimensional equation of motion

$$\nabla^4 w + w_{,\tau\tau} + CDw_{,\tau} = \lambda^2\alpha^{1/2}\nabla^2 f + \frac{\alpha}{x}\{f_{,x}(\hat{w} + w_s + w)_{,x} + f_{s,x}w_{,x}\}_{,x} + \frac{4\lambda^4}{\alpha^{1/2}}F(\tau) \tag{18a}$$

and the associated compatibility equation

$$\nabla^4 f = -\lambda^2\alpha^{-1/2}\nabla^2 w - \frac{1}{x}\{w_{,x}w_{,xx} + [(w_{,x} + w_{s,x})w_{,x}]_{,x}\}, \tag{18b}$$

where

$$\tau = t/\gamma, \quad \mathrm{CD} = \gamma c/\rho h, \quad \Omega = \gamma\omega \tag{19}$$

and $\gamma^2 = (\alpha a^4\rho/Eh^2)$ and ρ is the mass density. Here, t is time, ω is the driving frequency and c is the damping coefficient and τ, Ω and CD are the corresponding non-dimensional quantities.

The incremental state is assumed in the separable form

$$w(x,\tau) = \sum_{i=1}^{\mathrm{ND}} W_i(\tau)\phi_i(x), \tag{20a}$$

$$f(x,\tau) = \sum_{i=1}^{\mathrm{ND}} F_i(\tau)\psi_i(x). \tag{20b}$$

The substitution of expressions (20) into Eqs. (18a) and (18b), the use of the complete equations for the basic non-linear static state, and the application of the Galerkin method yields the following set of 2ND non-linear equations characterizing the dynamic behavior of the pre-loaded cap

$$
\begin{aligned}
&(W_{k,\tau\tau} + \mathrm{CD}W_{k,\tau})\{A(K_k) + B(K_k) - 3(J_1(K_k)B(K_k)/K_k)\} + W_k K_k^4/2\{A(K_k) - [2J_1(K_k)B(K_k)/K_k]\} \\
&\quad + \bar{F}_k\{[(2\lambda^4 + K_k^4)/2]A(K_k) - [J_1(K_k)(3\lambda^4 + 2K_k^4)B(K_k)/K_k] + (\lambda^4 + K_k^4)C(K_k)\} \\
&\quad + \sum_{\substack{i=1 \\ (i\neq k)}}^{\mathrm{ND}} \{\{2W_i K_k^3 K_i^3[K_i J_1(K_k)B(K_i) - K_k J_1(K_i)B(K_k)]/(K_k^4 - K_i^4)\} + F_1\{[2\lambda^4 + K_k^3[J_1(K_k)B(K_1) \\
&\quad - (K_k/K_i)J_1(K_i)B(K_k)]/(K_k^4 - K_i^4)] + (\lambda^4 + K_i^4)B(K_i)[B(K_k)/2 - 2J_1(K_k)/K_k]\}\}A_f[4\lambda^4\alpha^{-1/2}] \\
&\quad \times [2J_1(K_k)/K_k - B(K_k)/2]F(\tau) + \sum_{i=1}^{\mathrm{ND}}\sum_{j=1}^{\mathrm{ND}} \alpha^{1/2}\lambda^2 W_1 \bar{F}_j K_i \alpha_{ijk} + \sum_{i=1}^{\mathrm{NI}}\sum_{j=1}^{\mathrm{ND}} \alpha^{1/2}\lambda^2 \hat{W}_i \bar{F}_j K_i \alpha_{ijk} \\
&\quad + \sum_{i=1}^{\mathrm{NS}}\sum_{j=1}^{\mathrm{ND}} \alpha^{1/2}\lambda^2 W_{0i} \bar{F}_j K_i \alpha_{ijk} + \sum_{i=1}^{\mathrm{ND}}\sum_{j=1}^{\mathrm{NS}} \alpha^{1/2}\lambda^2 W_i \bar{F}_{0j} K_i \alpha_{ajk} = 0; \quad k = 1, \mathrm{ND},
\end{aligned} \tag{21}
$$

$$
\begin{aligned}
&(\bar{F}_k - W_k)\{[(2\lambda^4 + K_k^4)A(K_k)/2] + (\lambda^4 + K_k^4)C(K_k) - [(3\lambda^4 + 2K_k^4)J_1(K_k)B(K_k)/K_k]\} \\
&\quad + \sum_{\substack{(i=1) \\ (i\neq k)}}^{\mathrm{ND}} (\bar{F}_i - W_i)\{(\lambda^4 + K_k^4)B(K_k)[B(K_i)/2 - 2J_1(K_i)/K_i] + \{2\lambda^4 K_i^3[J_1(K_k)K_i B(K_i)/K_k \\
&\quad - J_1(K_i)B(K_k)]/(K_k^4 - K_i^4)\}\} + \sum_{i=1}^{\mathrm{ND}}\sum_{j=1}^{\mathrm{ND}} \alpha^{1/2}\lambda^2 W_1 W_j K_i K_j^2 \beta_{ijk}/K_k^2 + \sum_{i=1}^{\mathrm{NI}}\sum_{j=1}^{\mathrm{ND}} \alpha^{1/2}\lambda^2 \hat{W}_i W_j K_i K_j^2 \beta_{ijk}/K_k^2 \\
&\quad + \sum_{i=1}^{\mathrm{ND}}\sum_{j=1}^{\mathrm{NI}} \alpha^{1/2}\lambda^2 W_i \hat{W}_j K_i K_j^2 \beta_{ijk}/K_k^2 + \sum_{i=1}^{\mathrm{NS}}\sum_{j=1}^{\mathrm{ND}} \alpha^{1/2}\lambda^2 W_{0i} W_j K_i K_j^2 \beta_{ijk}/K_k^2 \\
&\quad + \sum_{i=1}^{\mathrm{ND}}\sum_{j=1}^{\mathrm{NS}} \alpha^{1/2}\lambda^2 W_i W_{0j} K_i K_j^2 \beta_{ijk}/K_k^2 = 0; \quad k = 1, \mathrm{ND}.
\end{aligned} \tag{22}
$$

To study the non-linear behavior of the cap, these equations are reduced to the usual set of first order differential equations, which are numerically integrated using the fourth-order Runge–Kutta.

3. Numerical analysis and results

3.1. Static analysis

The geometrical and physical parameters of the cap obtained experimentally are $R = 49.74$ mm, $h = 0.75$ mm, $E = 10.9$ N/mm^2 and $v = 0.37$. Using these values, one obtains for increasing values of the base radius, a the geometrical parameter λ and the corresponding critical load (see Fig. 4).

Using in Eqs. (10) and (11) the number of terms NS necessary to achieve convergence of the non-linear static state, one derives a set of 2NS coupled non-linear algebraic equations, which are solved by the Newton–Raphson method together with path following strategies. The number of terms necessary to achieve convergence of the whole non-linear equilibrium path increases as the geometric parameter λ increases. Typical equilibrium paths for perfect and imperfect caps with $\lambda = 5$ and $\lambda = 10$ are shown in Figs. 5 and 6, respectively, where the variation of the load parameter $Q[= q/q_{\mathrm{cr}}]$ is plotted as a function of the central deflection of the cap. Also shown inset in Figs. 5 and 6 is the form of the geometric imperfection which has the same form as the first buckling mode of the perfect cap. Initially the behavior of the shell is

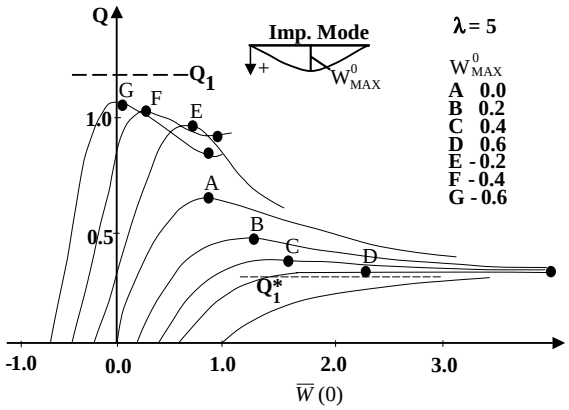

Fig. 5. Non-linear equilibrium paths for perfect and imperfect caps with $\lambda = 5$. Load parameter vs. normalized central deflection.

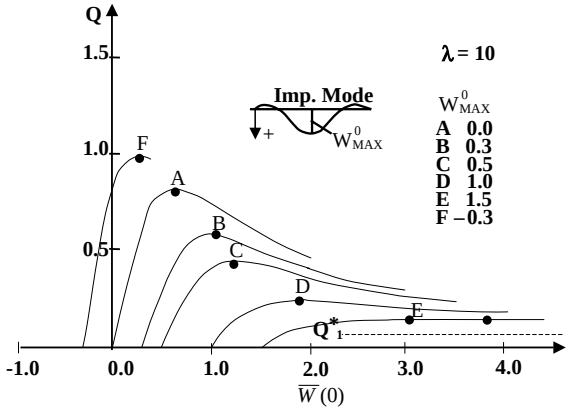

Fig. 6. Non-linear equilibrium paths for perfect and imperfect caps with $\lambda = 10$. Load parameter vs. normalized apex deflection.

practically linear and the load is supported mainly through membrane action. As the load increases the bending and the non-linear effects become more pronounced and the effective stiffness of the shell decreases and becomes zero at the upper limit point. Any further infinitesimal increase of the applied loading above the peak point value will produce a dynamic jump to a post-buckling configuration, with a large increase in deflection, characterizing the instability phenomenon known as snap-through buckling or limit-point instability. After the jump the shell presents any inverted configuration. If the load is increased still further, the shell will follow the ascending post-buckling path with increasing displacements and stresses. On the other hand, if the load is reduced slowly, the shell will follow the post-buckling path until the lower limit point is reached and then jumps back to a pre-buckling configuration. The descending branch of the equilibrium path is unstable and can never be reached under load control (VAD case). So, even though the structure is perfectly elastic, it exhibits hysteresis. It is this hysteretic cycle the responsible for the desired behavior of the VAD. Due to increasing pressure in the pneumatic chamber the shell jumps to the inverted position and deforms ejecting the blood from the blood chamber. Then, the pneumatic pressure decreases and the shell jumps back to a pre-buckling configuration, allowing the blood to fill the blood chamber again. As observed here, the variation of the pneumatic pressure must be carefully designed so that the difference between blood and pneumatic pressure will give rise to the desired hysteretic cycle not only in normal conditions but also in extreme case; for example, a person with high blood pressure.

As observed here, the cap is highly sensitive to initial geometric imperfections and the buckling load can be much lower or even higher then the limit point load of the perfect cap. However, a detailed parametric study considering different forms of imperfection and varying imperfection magnitude has shown that the critical load of the perfect cap has an upper bound Q_1 and a lower bound Q_1^* as indicated by dotted lines in Fig. 5. The upper bound is only slightly higher than the classical critical load of a complete spherical shell, q_{cl}. The lower bound can be closely approximated by the following expression deduced by Gonçalves and Croll (1992), using the reduced stiffness method:

$$Q_1^* = (7.34/\lambda^2). \tag{23}$$

Since the actual imperfections are not known a priori, the experimental buckling load may lay anywhere between these two values. In Fig. 7 a comparison of the scatter of previous experimental results in the usual range of λ is compared with the classical load parameter ($Q = 1$), the limit point load of the perfect cap, Q_U, and the lower bound given by Eq. (23). Also shown in this figure are the limit point loads obtained for imperfect shells with maximum imperfection amplitude equal to the shell thickness ($W^0_{MAX} = 1.0$) and half of the shell thickness ($W^0_{MAX} = 0.5$). As observed here, even moderate imperfections of the order of the shell thickness are enough to induce buckling at a load close to that associated with the lower bound. So, care should be taken in the construction of the VAD membrane to reduce the imperfections to a minimum. An experimental analysis of each membrane is also advisable to verify the load carrying capacity of each specimen. This will help in tuning the VAD pressure loading.

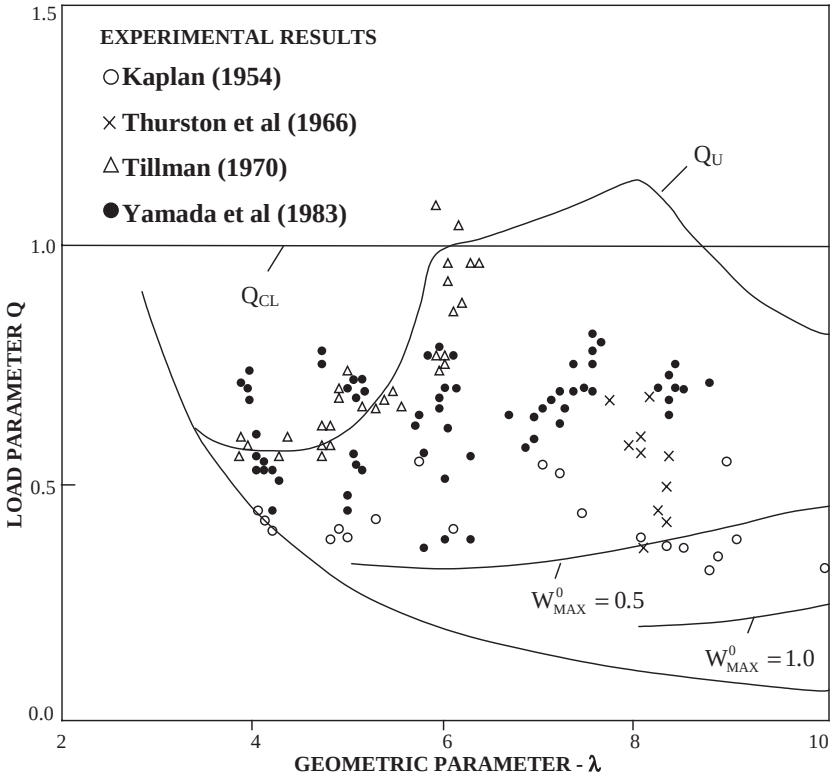

Fig. 7. Comparison of theoretical critical loads with previous experimental results.

3.2. Dynamic behavior under step load

If the pneumatic pressure is applied suddenly to the membrane, inertial effects will play and important whole in the VAD buckling behavior. As a first step in the VAD dynamic analysis, the response of the cap to a suddenly applied step load will be considered. The dynamic buckling of structures under step loads has been the subject of several papers in the past and recently various criteria have been proposed to evaluated the critical load of such structures using the tools of modern non-linear dynamics (Kounadis and Raftoyiannis, 1990; Dinkler and Kröplin, 1991). Fig. 8 shows the experimentally obtained results of the loading and unloading process of the membrane. As observed here, as a first approximation, the load acting on the cap can be modeled as a step load of finite duration. Fig. 9 shows the time response of a membrane

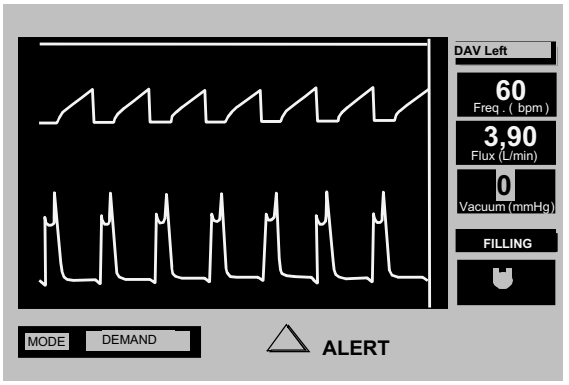

Fig. 8. Experimentally obtained data on the membrane loading and unloading processes.

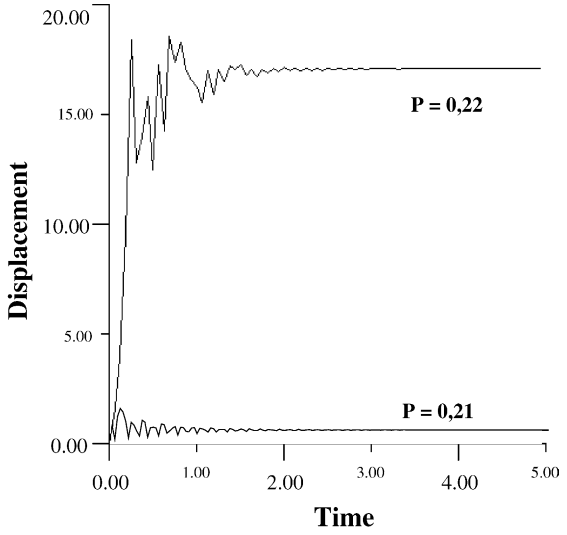

Fig. 9. Time response of a cap under a suddenly applied load of infinite duration ($\lambda = 8$).

with $\lambda = 8$ for two very close values of the step load parameter (0.21 and 0.22). For $Q = 0.21$, after a short transient the response converge to the unbuckled equilibrium position. For $Q = 0.22$, after the build-up of the response, the system escapes from the pre-buckling well and is directed to the post-buckling equilibrium configuration. The occurrence of the snapping phenomenon is revealed by the divergence of the response just after the application of the load. Hence the critical value of the dynamic buckling or escape load lies between these two values. The variation of the shell apex maximum response as a function of the load amplitude is shown in Fig. 10. One can observe that the maximum displacement increases slowly until the critical value is reached after which the shell exhibits a large jump to an inverted position. After buckling the apex displacement increases slowly again with increasing load. This feature is very important to the VAD behavior. If an un-reinforced membrane were used, it would certainly present large deformations under these loading conditions and would eventually touch the rigid blood chamber, causing hemolysis, i.e., the breakdown of red blood cells. Some processes such as the incorrect VAD behavior or, for example, hemodialysis and the use of heart-lung bypass machines can cause pre-mature breakdown of red blood cells and leave fewer than normal red cells available for oxygen transport. To prevent large deformations after buckling, the cotton net was included between two polyurethane skins. Being the deformations small, the total volume of blood displaced by the membrane during the snap through process is approximately given by:

$$V_b = \frac{2}{3}\pi H^2(3R - H), \tag{24}$$

where $H = R - \sqrt{R^2 - a^2}$ is the apex height.

The dynamic bucking load is, due to inertial effects, much lower than the static buckling load for any value of λ, as shown in Fig. 11 where the VAD critical loads under static and step load are plotted as a function of the geometrical parameter λ. So, a much lower pressure and, consequently, less potent pump is needed for the perfect functioning of the VAD. The influence of the damping parameter is illustrated in Fig. 12 where the variation of the critical load with λ is plotted for increasing values of the damping parameter CD. Although damping has a small increasing effect on the critical step load, it has a beneficial

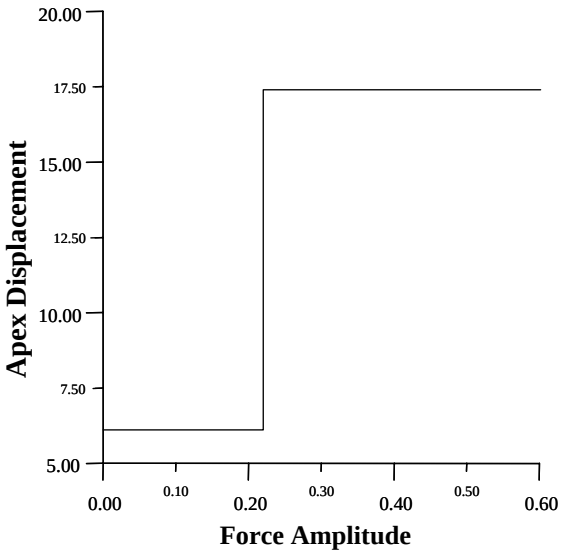

Fig. 10. Variation of shell apex displacement as a function of the step load amplitude.

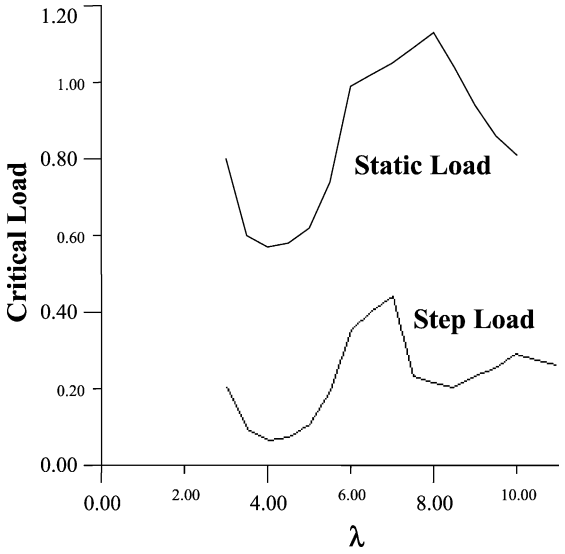

Fig. 11. Critical load as a function of the geometrical parameter λ. Shell under static and suddenly applied load (step load).

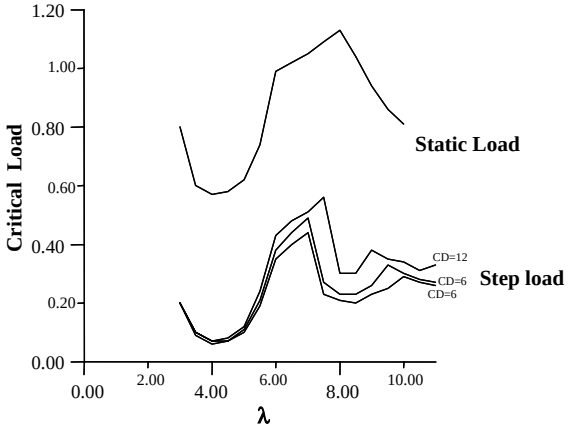

Fig. 12. Influence of the viscous damping parameter on the dynamic buckling load.

effect on the VAD dynamic response diminishing the length and maximum amplitude of the transient response after buckling (see Fig. 9) and consequently undesirable pressure fluctuations. The total damping due to the membrane material and the blood that acts as a viscous damper leads in practice to a high damping ratio, which is beneficial to the VAD behavior.

Another factor that has an important influence on the VAD behavior is the static pre-loading. If the mean pressure in the pneumatic chamber between two loading steps does not go to zero, the remaining pressure Q_S may decrease noticeably the critical value of the step (added) load in each step, as shown in Fig. 13 where the critical step load is plotted for two values of static pre-loading: 10% and 50% of the corresponding static critical load.

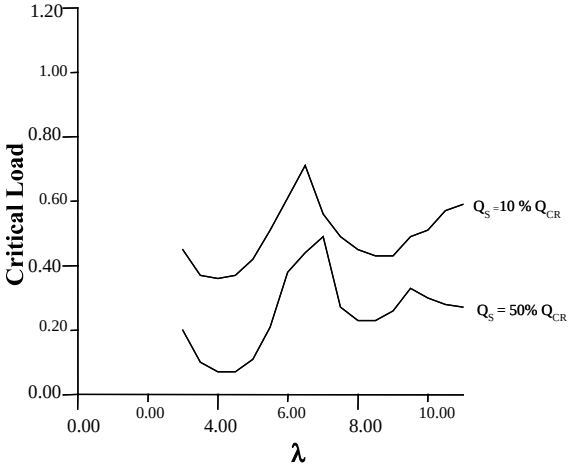

Fig. 13. Influence of static pre-loading on the VAD dynamic buckling load.

3.3. Dynamic behavior under harmonic load

As the loading and unloading process continues, the cap exhibits large cross-well motions due to the action of this periodic load. As a further step in the understanding of the VAD dynamic behavior, the behavior of the cap under harmonic load was analyzed. The shell under uniformly distributed pressure loading is considered to be initially at rest in a potential well corresponding to a pre-buckling configuration. Then harmonic excitation is applied and conditions for escape from this potential well are sought. Fig. 14 shows a typical bifurcation diagrams for a shallow shell with $\lambda = 4$ under harmonic loading ($F\sin(\omega t)$) with the excitation frequency in the vicinity of the lowest natural frequency of the shell. Fig. 14(a) shows a bifurcation diagram for a forcing frequency parameter $\Omega = 9$ while Fig. 14(b) show the results for $\Omega = 13$. The forcing amplitude is used as the control parameter. In Fig. 14(a), initially, for small forcing amplitudes, the shell exhibits a period one small amplitude response within the pre-buckling well. As the load increases the shell reaches a point where a sub-critical bifurcation occurs and the period-one stable solution becomes unstable. At this point the shell jumps into the post-buckling well and exhibits a period one small amplitude response around the static post-buckling configuration. As the load increases still further the shell exhibits a period doubling cascade, large amplitude chaotic cross-well motions, a window of period three and chaotic motions again. In Fig. 14(b), the bifurcation point corresponds to a super-critical bifurcation of the period one solution, giving rise to a period-two stable solution which is followed by a period doubling cascade eventually reaching the escape boundary where the solution jumps to the post-buckling well. These non-linear behaviors may cause serious disturbances in the blood flow and should be avoided for the safety of the mechanical device and, more important, the safety of the patient. The periodic load applied to the VAD must have such a period and magnitude so that the membrane will exhibit period one large cross-well motions. A refined parametric analysis in the control parameters space is therefore necessary to ensure the correct behavior of the VAD and the desired blood flow. A detailed parametric analysis was then conducted where, for several values of λ ranging from very shallow to moderately deep caps, the dynamic response of the cap was analyzed using bifurcation diagrams, Poincaré maps and time responses and having as control variables the frequency and forcing amplitude. A typical escape boundary in the force control space is shown in Fig. 15. This curve was obtained by increasing slowly the amplitude while holding the frequency constant. The response of the spherical cap is found to be, in many respects, similar to the response of a soft non-linear spring under harmonic load (Soliman, 1993; Soliman and

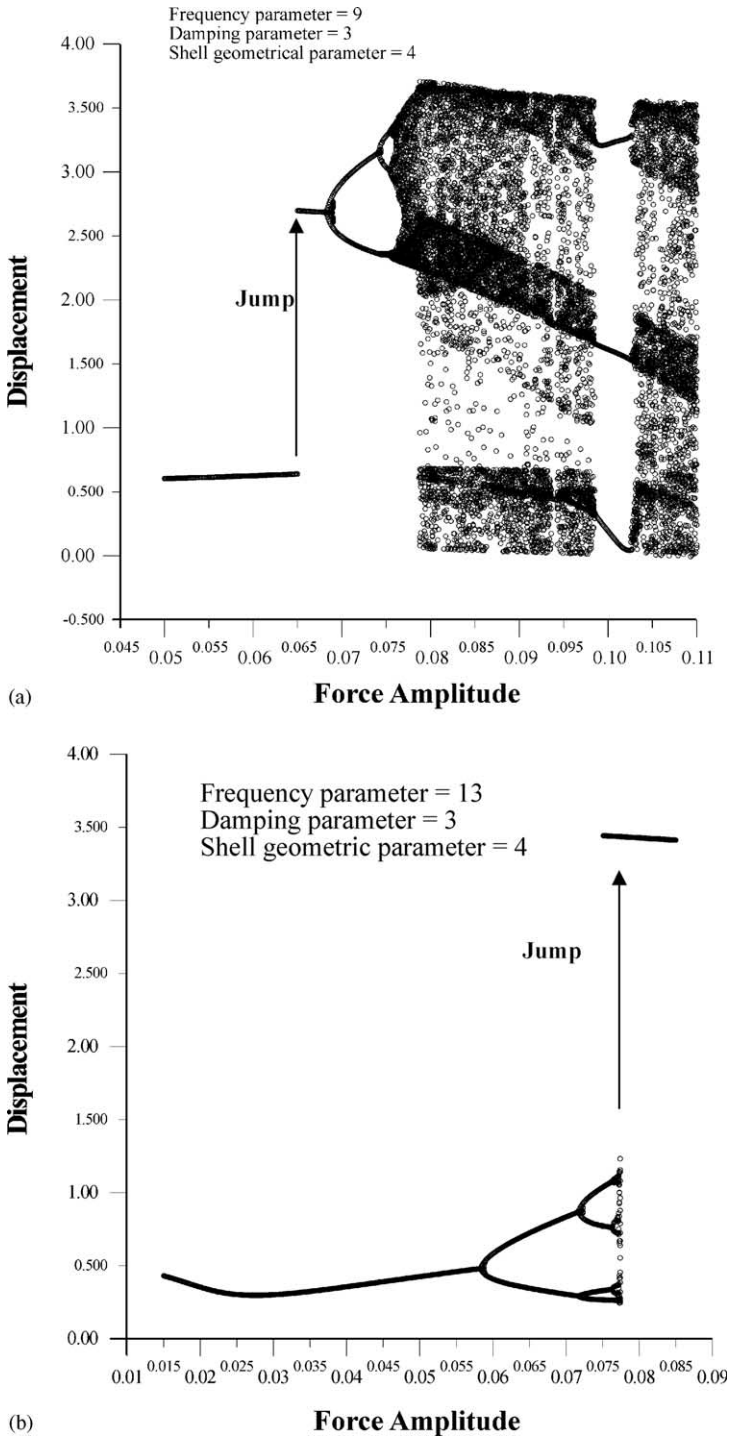

Fig. 14. Bifurcation diagram—shell under harmonic forcing. (a) Sub-critical bifurcation. (b) Super-critical bifurcation.

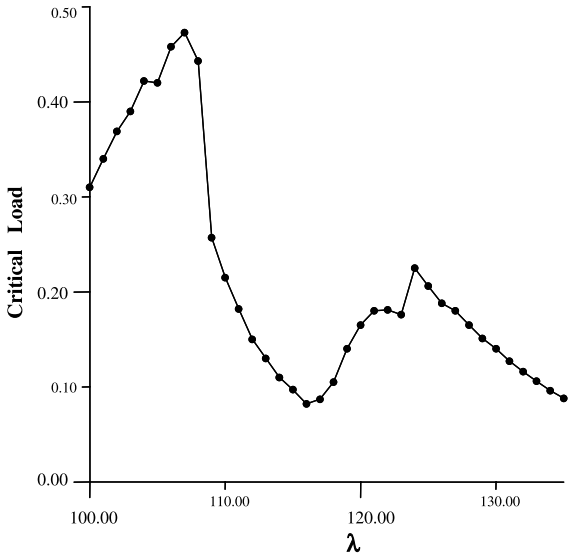

Fig. 15. Stability boundary in control space (forcing frequency vs. forcing amplitude) $\lambda = 10$.

Gonçalves, 2003); the descending branches of the stability boundary are associated with sub-critical bifurcations while the ascending branches are associated with super-critical bifurcations of the basic period one response. For such sub-critical bifurcations the stability of the basic period one solution is suddenly lost and the system jumps in search of another stable solution. For a super-critical bifurcation, the shell response exhibits a period-doubling cascade just before escape. The softening characteristics of the cap was previously identified by Gonçalves (1994), among others, using a multi-degree-of-freedom model and the Galerkin-Urabe method.

For very shallow shells under uniform pressure loading, both the static and dynamic responses are always axi-symmetric. As the value of the geometrical parameter λ increases, the non-linear behavior becomes very sensitive to even very small asymmetries in the loading and/or geometry and non-symmetric effects can no longer be disregarded in the analysis. This is an on-going research project and future steps will include a precise experimental measurement of the loading forces so that a more precise modeling of the load may be used in the theoretical analysis. Another step is to include non-symmetric effects in the dynamic analysis. The influence of non-symmetric effects on the static response of the cap was already studied using the finite element software ABAQUS (Teixeira et al., 2001) and results shows that for moderately deep caps the buckling load is highly sensitive to non-symmetric loading and geometric imperfections, but the lower bound is always given by Eq. (23). Nonetheless, the present results already gives a clear idea of the VAD static and dynamic non-linear behavior and stability and provides a basis for the development of a safe and reliable VAD.

4. Conclusions

In the present research Marguerre shallow shell equations were used to analyze the non-linear dynamic behavior of the VAD–InCor membrane. The non-linear axisymmetric behavior of the shell under dynamic pressure loading was analyzed under different types of loading relevant to the problem, in particular, step and periodic loads. The results show that the shell response is highly sensitive to geometric imperfections

and to the geometric parameter λ. Also, when periodic loads are applied the results are highly dependent on the load control parameters such as period and force amplitude. As one of the control parameters is varied the shell may display a wealth of non-linear phenomena including chaotic motions, jumps and sub-harmonic oscillations of various orders. Many of these non-linear behaviors may cause serious disturbances in the blood flow and should be avoided for the safety of the mechanical device and, more important, the safety of the patient. So, in order to ensure the perfect functioning of the VAD a detailed parametric analysis must be conducted covering the whole control parameter space relevant to the problem. For very shallow shells the response is axisymmetric, as the geometric parameter λ increases, non-symmetric effects must be included in the formulation of the problem. Future work will consider the influence of non-symmetric geometric imperfections and loading on the mechanical behavior of the VAD.

References

Abramovitz, M., Stegun, I.A., 1964. Handbook of Mathematical Functions. Dover, New York.

Budiansky, B., Hutchinson, J.W., 1964. Dynamic buckling of imperfection-sensitive structures. In: Proceedings of the Eleventh International. Congress of Applied Mechanics, Munich, Germany.

Budiansky, N., Roth, R.S., 1962. Axisymmetric dynamic buckling of clamped shallow spherical shells. In: Collected Papers on Instability of Shell Structures, NASA TND-1510, pp. 597–606.

Dinkler, D., Kröplin, B., 1991. An energy based concept for dynamic stability of elastic structures. In: Jullien, J.F. (Ed.), Buckling of Shell Structures on Land, in the Sea and in the Air. Elsevier, London, pp. 83–91.

Dumir, P.C., Gandhi, M.I., Nath, Y., 1984. Axisymmetric static and dynamic buckling of orthotropic shallow spherical caps with flexible supports. ACTA Mechanica 52, 93–106.

Gonçalves, P.B., 1994. Axisymmetric vibrations of imperfect shallow spherical caps under pressure loading. J. Sound and Vibration 174 (2), 249–260.

Gonçalves, P.B., 1999. The complex non-linear dynamics of imperfection sensitive shells. In: Moon, F.C. (Ed.), IUTAM Symposium on New Applications of Nonlinear and Chaotic Dynamics in Mechanics. Kluwer Academic Publishers, Dordrecht, The Netherlands.

Gonçalves, P.B., Croll, J.G.A., 1992. Axisymmetric buckling of pressure-loaded spherical caps. ASCE J. Structural Engng. 118, 970–985.

Hibbitt, Karlsson, Sorensen, Inc., ABAQUS Software:version 5.8:1998.

Huang, N.C., 1969. Axisymmetric dynamic snap-through of elastic clamped shallow spherical shells. AIAA J. 7 (2), 215–220.

Kounadis, N.A., Raftoyiannis, J., 1990. Dynamic stability criteria of nonlinear elastic damped/undamped systems under step loading. AIAA J. 28 (7), 1217–1223.

Leiner, A.A., Moreira, L.F.P., Stolf, N.A.G., 1998. Assistência Circulatória Mecânica: Aspectos Atuais. Revista da Sociedade de Cardiologia do Estado de São Paulo 8 (3), 464–475.

Marguerre, K., 1939. Zur Theorie der gekrümmten platte grosser formänderung. Jahrbuch der 1939 der deustchen Luftfahrforschung, p. 413.

Sezai, Y., 2001. Progress and future perspectives in mechanical circulatory support. Artificial Organs 25 (5), 318–322.

Simitses, G.J., 1974. On the dynamic buckling of shallow spherical caps. J. Appl. Mech. 41 (1), 299–300.

Soliman, M.S., 1993. Jumps to resonance: long chaotic transients, unpredictable outcome, and the probability of restabilization. J. Appl. Mech. 60, 669–676.

Soliman, M.S., Gonçalves, P.B., 2003. Chaotic behavior resulting in transient and steady-state instabilities of pressure-loaded shallow spherical shells. J. Sound and Vibration 259 (3), 497–512.

Teixeira, P.B.C., 2001. Mechanical Behavior and Stability of the Internal Membrane of the InCor Ventricular Assist Device (In Portuguese), M.Sc. Thesis, Civil Engineering Department, PUC-Rio, Brazil.

Teixeira, P.B.C., Pamplona, D., Gonçalves, P.B., Cestari, I., Leirner, A., 2001. Mechanical behavior and stability of the internal membrane of the InCor ventricular assist device. Artificial Organs 25, 912–921.

Thompson, J.M.T., 1989. Chaotic phenomena triggering the escape from a potential well. Proceedings of Royal Society of London A 421, 195.

Tillman, S.C., 1970. On the buckling behavior of shallow spherical caps under uniform pressure load. Int. J. Solids and Structures 6, 37–52.

Virgin, L.N., Plaut, R.H., Cheng, C.C., 1992. Prediction of escape from a potential well under harmonic excitation. Int. J. Non-Linear Mech. 27 (3), 357–365.

Yamada, S., Uchiyama, K., Yamada, M., 1983. Experimental investigation of the buckling of shallow spherical shells. Int. J. Non-Linear Mech. 18, 37–54.
Yasuda, K., Kushida, G., 1984. Nonlinear forced oscillations of a shallow spherical shell. Bull. JSME 27, 2233–2240.